Climate Dynamics (2024) 62:2499–2515
https://doi.org/10.1007/s00382-023-07035-8

ORIGINAL ARTICLE

# Statistical relationships between the Interdecadal Pacific Oscillation and El Niño–Southern Oscillation

Hanna Heidemann[1,2,3] · Tim Cowan[2,4] · Scott B. Power[2,3,5,9] · Benjamin J. Henley[6,7,8]

Received: 13 July 2023 / Accepted: 20 November 2023 / Published online: 26 December 2023


## Abstract

The climate of the Pacific Ocean varies on interannual, decadal, and longer timescales. This variability is dominated by the El Niño–Southern Oscillation (ENSO) and the Interdecadal Pacific Oscillation (IPO), both of which have profound impacts on countries within and well beyond the Pacific. To date, previous studies have only examined a small subset of the possible links between ENSO, its diversity, and the IPO. Here we focus on the statistical relationship between decadal variability in ENSO properties and the IPO, testing the null hypothesis that the IPO arises from random decadal changes in ENSO activity, including ENSO diversity. We use observed sea surface temperature (SST) records since 1920 to investigate how the timing, structure, frequency, duration, and magnitude of El Niño and La Niña events differ between IPO phases. We find that using the relative frequency of El Niño and La Niña events and either the mean event duration or SST magnitude can reproduce up to 60% of the IPO Tripole Index timeseries. While the spatial SST patterns that represent the IPO and ENSO are similar, the IPO is meridionally broader in the central to eastern Pacific, which may be caused by a lagged relationship with low-frequency SST variability in the equatorial Pacific. In addition, North Pacific SST anomalies of opposite sign to the tropical Pacific SST anomalies is a unique feature of the IPO that cannot be explained by decadal ENSO variability. This suggests a clear IPO and ENSO relationship, but also independence in some of the IPO's characteristics.

**Keywords** Climate variability · El Niño–Southern Oscillation · Interdecadal Pacific Oscillation · Sea surface temperature

## 1 Introduction

The spatiotemporal diversity of El Niño–Southern Oscillation (ENSO) exhibits variability on decadal timescales (e.g. Timmermann et al. 2018; Capotondi et al. 2020; Dieppois et al. 2021). Such ENSO characteristics include the magnitude of equatorial and off-equatorial sea surface temperature anomalies (SSTa), the zonal location of the SST maxima and the relative frequency of El Niño events, both central Pacific (CP) and eastern Pacific (EP) types, and La Niña events (e.g. Timmermann 2003; Power and Smith 2007; Freund et al. 2019; Power et al. 2021). While a comprehensive understanding of the causes of decadal changes in ENSO characteristics is yet to be provided (Power et al. 2021), it is hypothesised that stochastic variability in the atmosphere and ocean (Power et al. 2006), decadal variability in surface

✉ Hanna Heidemann
Hanna.Heidemann@unimelb.edu.au

Tim Cowan
Tim.Cowan@bom.gov.au

Scott B. Power
scott.power@monash.edu.au

Benjamin J. Henley
bhenley@uow.edu.au

[1] School of Geography, Earth and Atmospheric Sciences, University of Melbourne, Parkville, Australia

[2] Centre for Applied Climate Sciences, University of Southern Queensland, Toowoomba, Australia

[3] ARC Centre of Excellence for Climate Extremes, Monash University, Clayton, Australia

[4] Bureau of Meteorology, Melbourne, Australia

[5] School of Earth, Atmosphere and Environment, Monash University, Clayton, Australia

[6] Securing Antarctica's Environmental Future, University of Wollongong, Wollongong, Australia

[7] School of Earth, Atmospheric and Life Sciences, University of Wollongong, Wollongong, Australia

[8] Department of Infrastructure Engineering, University of Melbourne, Parkville, Australia

[9] Climate Services International, Oakleigh, Australia

and subsurface ocean processes and wind stress (England et al. 2014), and natural and anthropogenic external forcing all play a role (Timmermann et al. 2018; Power et al. 2021).

Pacific variability on a 10 to 30-year timescale is associated with the Pacific Decadal Oscillation (PDO) in the North Pacific (Mantua and Hare 2002) or the basin-wide Interdecadal Pacific Oscillation (IPO; Power et al. 1999). Even though the PDO is defined using North Pacific SSTs and the IPO defined using either Pacific-wide Empirical Orthogonal Function (EOF) analysis or the IPO Tripole Index (TPI), their temporal evolution and their Pacific-wide SST patterns are very similar (Han et al. 2014). Warm (positive) and cool (negative) IPO periods have been identified as a cause for decadal variability in global mean surface temperatures (Maher et al. 2014), including the warming hiatus in the early 2000s (England et al. 2014). The extent to which the IPO is influenced by decadal changes in ENSO characteristics or whether the IPO modifies ENSO and its related atmospheric teleconnections, is the subject of ongoing research. Studies have concluded that random changes in ENSO activity alone can potentially explain some of the IPO variability (Power and Colman 2006; Power et al. 2006, 2021).

The IPO may be the result of numerous Pacific-wide compounding mechanisms that involve both the ocean and atmosphere as well as tropical-extratropical teleconnections (Newman et al. 2016). These firstly include processes such as tropical Pacific decadal SST variability, tropical-extratropical ENSO teleconnections and coastally trapped oceanic Kelvin waves that propagate from the equator to high latitudes along the eastern ocean boundaries. Secondly, stochastic atmospheric forcing contributes to Pacific decadal variability. This includes fluctuations of the Aleutian Low (Newman et al. 2016), as well as variability in the subtropical-tropical overturning cells which can be due to changes in tropical or extratropical winds and subduction of subtropical water. These wind-driven overturning circulations modify equatorial upwelling (McCreary and Lu 1994). Variability of the trade winds is associated with the North and South Pacific meridional modes. While Liguori and Di Lorenzo (2019) suggest that the South Pacific meridional mode is more important for tropical Pacific decadal variability than its northern counterpart, other studies emphasise the importance of the North Pacific meridional mode for tropical Pacific decadal variability (Di Lorenzo et al. 2015; Capotondi et al. 2022; Newman et al. 2016). The meridional modes have been connected to the broadening of the SST pattern at the decadal timescale compared to the interannual ENSO pattern (Zhang et al. 2014; Liguori and Di Lorenzo 2019). Further processes include the 're-emergence mechanism' in the midlatitudes such as upper ocean memory of persistent temperature anomalies over consecutive years (Alexander et al. 1999) and decadal variability in summertime low-level cloudiness in the North Pacific. Lastly, low-frequency variability in heat transport associated with the Kuroshio-Oyashio Extension is likely an important part of Pacific decadal variability (Newman et al. 2016; Zhao et al. 2021; Di Lorenzo et al. 2023). In addition, both anthropogenic and natural external forcings, such as greenhouse gases, volcanic eruptions and aerosol changes (Qin et al. 2020), have been identified as potential factors that influence Pacific decadal variability (Power et al. 2021).

Transitions from negative to positive phases of the IPO are thought to be triggered by off-equatorial build-up of upper ocean (above the 20 °C isotherm) heat content in the western Pacific, followed by the occurrence of a strong El Niño (Meehl et al. 2021). The opposite is true for a positive to negative IPO phase transition, which can be triggered by negative ocean heat content anomalies in the off-equatorial western Pacific, followed by the build-up of a strong La Niña event (Meehl et al. 2021; Gordon et al. 2021). However, the predictability of decadal variability in the Pacific is still limited, as shown for the PDO by Choi and Son (2022) in decadal hindcasts from seasonal-to-decadal prediction systems as part of Coupled Model Intercomparison Project phase 5 (CMIP5) and phase 6 (CMIP6). The complexity and ambiguity of proposed contributing mechanisms to the decadal variability in the Pacific Ocean pose a challenge for predicting it.

While a strong similarity between the low-pass filtered ENSO signal and the IPO has been shown in a coupled climate model (Power et al. 2006), this relationship is still to be shown in the latest generations of CMIP6 climate models. In observations, the ENSO and IPO SSTa patterns are very similar (Vimont 2005), especially when the lagged evolution of ENSO is taken into account (Vimont 2005; Power et al 2021). One main difference is that the IPO pattern is meridionally broader near the equator. This was shown in a climate model to be partly due to the fact that the oceanic response to ENSO-driven fluxes of heat and wind-stress gives rise to linkages between equatorial and off-equatorial SST variability that are stronger on multi-year to decadal timescales (Power and Colman 2006). More recently, Power et al. (2021)—using the method described by Vimont (2005)—showed a strong similarity between the El Niño pattern, averaged over 2 years, and the tropical decadal variability pattern. However, this research did not analyse if any differences in the SST patterns exist between positive IPO (IPO +) and negative IPO (IPO −) phases. Therefore, we will address this in the current study.

The aim of this paper is to provide a wide-ranging examination of the statistical links between observed variability linked to the IPO, ENSO, and ENSO diversity. We will first investigate whether there are decadal differences in ENSO event characteristics such as event timing, duration, frequency, structure, and magnitude. We will secondly evaluate

mean characteristics of the IPO and will finally assess the statistical links between both ENSO and the IPO. We will test the simplest null hypothesis ($H_0$): The IPO is a statistical residual of decadal variations in ENSO activity including ENSO diversity. An alternative more sophisticated null hypothesis ($G_0$) is that some of the IPO's variability arises as a lagged response to surface fluxes of heat and momentum that is partially driven by ENSO (Power and Colman 2006; Power et al. 2021). Note that this is a statistical study, so the test is not definitive. It will, nevertheless, highlight relationships that are, or are not, readily explained by $H_0$ and $G_0$. These issues will be addressed further in the discussion section.

In the following sections we describe the data and methods applied, followed by the results. This includes an overview of the decadal variability in ENSO characteristics and the statistical relationship they have with the IPO. In the final section, we discuss how the results support or reject $H_0$ and $G_0$.

## 2 Data and methods

We use observed gridded SST data for January 1920 to April 2022 from the Hadley Centre Global Sea Ice and Sea Surface Temperature version 1.1 (HadISST v1.1) dataset (Rayner et al. 2003). The analysis is not extended further back in time to 1870 (which is the start year available for HadISST v1.1) due to constraints in SST data quality in the tropical Pacific prior to the 1920s (Deser et al. 2010).

A range of SST indices are considered, which characterise SST variability in the tropical and extratropical Pacific: the Niño 3 (5 N–5° S, 150°–90° W), Niño 4 (5° N–5° S, 160° E–150° W) and Niño 3.4 (5° N–5° S, 170° W–120° W) indices for interannual and the TPI for decadal timescales. The TPI uses Pacific SSTa in the tropical region (10° S–10° N, 170° E–90° W) as well as SSTa in the north (25° N–45° N, 140° E–145° W) and southwest Pacific (50° S–15° S, 150° E–160° W; Henley et al. 2015). While the TPI is characterised by a significant ($p < 0.05$) negative linear trend of − 0.03 °C per decade from 1920 to 2022, the Niño 4 index shows a significant ($p < 0.05$) warming trend in the central Pacific at + 0.03 °C per decade, whereas the eastern Pacific (Niño 3) has warmed by + 0.02 °C per decade. In the following, and throughout this study, the SSTa are calculated relative to the 1981 to 2010 climatology and all results based on SST are linearly detrended over the period 1920 to 2022 (April).

Central Pacific (CP) and eastern Pacific (EP) El Niño events are defined using the eastern Pacific/cold tongue (EP) and central Pacific/warm pool (CP) indices by Ren and Jin (2011), as described in Heidemann et al. (2022). The ENSO indices are detrended and standardised prior to event definition and a 3-month moving average is applied. In this study, the duration of each ENSO event is the total number of consecutive months in which one standard deviation of the respective index is exceeded. The minimum duration of an event are three consecutive months above the threshold, to occur in or overlap with the extended austral summer season from September to the following March. Due to the similarities in atmospheric dynamics and SST patterns associated with EP and CP La Niña events, and due to a limited sample size of EP events (Heidemann et al. 2022), both types of La Niña events are pooled together in this analysis.

To examine decadal variability in the tropical and extratropical Pacific, we define the IPO phases using a 13-year low-pass filtered timeseries of the TPI, following Henley et al. (2015). The IPO + phases are found to be: 1924 to 1944 and 1977 to 1998, and IPO − phases: 1945 to 1976 and 1999 to 2014. The state of the IPO from 2015 to 2022 is undetermined and therefore excluded. Hence, all SSTa composites that refer to specific IPO + or IPO − phases use the time period 1924 to austral summer 2014/2015 and all other analysis uses the entire time period 1920 to 2022.

We calculate SSTa composites for EP and CP El Niño and all La Niña events and separate them based on IPO phase to determine if there are robust differences between the events during different IPO phases. As ENSO event composites are calculated relative to the mentioned threshold relative to the mean state, a caveat arises that the resulting composites may include both an interannual and decadal signal. To capture the evolution of the ENSO events, we examine 18-month composites from March (M) prior the peak of the event, to August (A + 1) after the event peak (M to A + 1). The significance of the composite SSTa patterns is computed using a Monte Carlo method, detailed in Heidemann et al. (2022). To detect any significant differences in the ENSO event characteristics between IPO + and IPO − phases, a two-sample t-test is applied (Wilks 2011).

We further evaluate seasonal SSTa profiles, which are meridionally averaged SSTa from 10° N to 10° S at each longitude in the equatorial Pacific region. The profiles are assessed for austral spring (September to November, SON), summer (December to February, DJF) and autumn (March to May, MAM) to analyse the decadal differences in the magnitude of equatorial SSTa around the peak of the event. Throughout the paper, we refer to austral seasons only.

To compare summer SSTa variability in the Pacific between interannual and decadal timescales, an EOF analysis is conducted with both unfiltered and 13-year low-pass filtered SSTa from 60° N to 60° S and 70° E to 60° W. To determine the statistical significance of the correlation coefficient from two low-pass filtered timeseries and hence account for autocorrelations, block bootstrapping is applied (Wilks 2011). For each summer season included in the low-pass filtered timeseries, blocks of 10 consecutive

observations in the analysed timeframe are randomly sampled (with replacement) 11 times to have at least as many block samples as values included in the original timeseries. These blocks are then used to create a new artificial timeseries made of the block bootstrapped samples. The Pearson correlation coefficient between two timeseries is then calculated, and the mean value of the statistic is saved. This process is repeated 10,000 times (e.g. Wilks 2011) to generate a probability density function of all randomly generated correlation coefficients. The critical value is then calculated, with the observed correlation value needing to be within the 5th percentile of the distribution (2.5th percentile on each end of the distribution; exceeding the critical value at both ends of the distribution) for the magnitude of the correlation coefficient to be considered statistically significant.

To compare ENSO and IPO SSTa patterns, pattern correlation coefficients are calculated using the area 60° N to 60° S and 70° E to 60° W. We further evaluate other basic statistics such as the standard deviation of SSTa at each grid point as a measure of variability in Pacific Ocean SSTs. Lag correlations between Niño 3.4 and grid point SSTa to the north, west and south of the Niño regions, with the specific locations shown in Fig. 6 are also calculated to identify the maximum lag between Niño 3.4 and SSTa in those regions.

Throughout the paper, statistical significance is defined using a threshold of $p < 0.05$ and the word 'significant' is only used in this context unless otherwise specified. For some more exploratory analysis that may not reach the 95th percentile threshold for significance but is nevertheless worth mentioning, we state the significance level at $p < 0.1$.

## 3 Results

We first explore characteristics of ENSO events based on large scale SSTa and the tropical Pacific SSTa indices. We will explore how the following ENSO event characteristics differ between IPO − and IPO + phases: ENSO event frequency, duration and timing in subsection 3.1, ENSO event SSTa structure and magnitude in subsection 3.2.

### 3.1 ENSO event frequency, duration and timing

Here we examine the frequency, duration and timing of CP El Niño, EP El Niño, La Niña events and ENSO neutral years during the two IPO + and two IPO − phases from 1920 to 2022. We also examine the statistical significance of the differences that arise in ENSO event frequencies between the two IPO phases.

The frequency of ENSO events and ENSO neutral years during IPO + and IPO − phases is summarised in Table 1. During IPO − phases, ENSO (CP El Niño, EP El Niño, La Niña) events occurred in 67% of years and the remainder (33%) were ENSO neutral. In contrast, in IPO + phases, ENSO events occurred in about half (49%) of all years. The clearest decadal difference in ENSO event frequency is evident for La Niña, as 19 La Niña events were recorded in IPO − phases and only six events in IPO + phases. Thus, over three times as many La Niña events have occurred in the IPO − phase compared to the IPO + phase. The remaining differences are small: seven CP El Niño events occurred in IPO − phases and five events in IPO + phases; and ten EP El Niño events occurred in IPO + phases, compared to seven events during IPO − phases.

The timing and event duration for each individual CP El Niño, EP El Niño and La Niña event, as well as the timing and duration averaged over all events and both IPO + and IPO − phases are shown in Fig. 1 and Table 1. CP El Niño events have a mean duration of 6 months regardless of IPO phase. However, there is a small difference in the start and end months: in IPO − phases, on average the CP El Niño events start 1 month earlier (October) than during IPO + phases. They also terminate earlier (April + 1) in IPO − phases than in IPO + phases (November to May; Fig. 1a).

On average, EP El Niño events last longer (10 months; July to May + 1) during IPO + phases compared to events during IPO − phases (7 months; June to January + 1, Fig. 1b, solid red and blue line). La Niña events typically have a duration of 7 months in IPO − phases and 9 months in IPO + phases, terminating in March and May, respectively. The start date for La Niña events in both IPO + and IPO − phases is the same (July, Fig. 1c, solid blue and red line). The negative SSTa develop earlier in IPO − phases than in IPO + phases, as the SSTa hover just below the La Niña threshold in the months preceding the event (Fig. 1c). The duration of CP El Niño, EP El Niño and La Niña events do not show any significant differences between IPO − and IPO + (Table 1).

### 3.2 ENSO event SSTa structure and magnitude

In this section, we evaluate the spatial structure (i.e., patterns) of 18-month averaged SSTa during CP El Niño, EP El Niño and La Niña events and how they differ between IPO − and IPO + phases (Fig. 2). We further evaluate zonal SSTa 'profiles' in the tropical Pacific, which are averaged over the equatorial region from 10° N to 10° S. This identifies any IPO phase-related differences in the magnitude of equatorial SSTa during the developing ENSO event in spring (SON), the peak in summer (DJF), and the event demise in the following autumn (MAM + 1); Fig. 3). The background shading in Fig. 3 (blue for IPO − and pink for IPO +) indicates the range of SSTa (including maximum and minimum) throughout the equatorial Pacific for each ENSO event type. We also assess the statistical significance of the IPO −/IPO + differences.

**Table 1** ENSO characteristics during IPO + and IPO − phases (1924–2015), and the statistical significance of the differences between them

| ENSO metric | IPO phase | CP El Niño | EP El Niño | La Niña | Neutral | Total |
|---|---|---|---|---|---|---|
| (1) Frequency (count [percentage of years]) | IPO − | 7 [14%] | 7 [14%] | 19 [39%] | 16 [33%] | 49 [100%] |
| | IPO + | 5 [12%] | 10 [23%] | 6 [14%] | 22 [51%] | 43 [100%] |
| (2) Duration (months) | IPO − | 6 | 7 | 7 | | |
| | IPO + | 6 | 10 | 9 | | |
| Level of significance for IPO −/IPO + differences | | p > 0.1 (not significant) | p > 0.1 (not significant) | p > 0.1 (not significant) | | |
| (3) Average event timing | IPO − | Oct–Apr | Jun–Jan | Jul–Mar | | |
| | IPO + | Nov–May | Jul–May | Jul–May | | |
| (4) Magnitude in eastern Pacific (°C) in DJF | IPO − | 0.23 | *0.62* | **− 0.71** | | |
| | IPO + | 0.17 | *1.12* | **− 0.38** | | |
| Level of significance for IPO −/IPO + differences | | p > 0.1 (not significant) | *p < 0.1* | **p < 0.05** | | |
| (5) Magnitude in central Pacific (°C) in DJF | IPO − | 0.67 | *0.52* | − 0.77 | | |
| | IPO + | 0.55 | *0.73* | − 0.85 | | |
| Level of significance for IPO −/IPO + differences | | p > 0.1 (not significant) | *p < 0.1* | p > 0.1 (not significant) | | |
| (6) Magnitude in North Pacific (°C) in DJF | IPO − | − 0.11 | **0.03** | ***0.49*** | | |
| | IPO + | 0.01 | **− 0.86** | **− 0.13** | | |
| Level of significance for IPO −/IPO + differences | | p > 0.1 (not significant) | **p < 0.05** | **p < 0.05** | | |
| (7) SST pattern difference between central Pacific and North Pacific (˚C) | IPO − | 0.77 | **0.49** | **− 1.26** | | |
| | IPO + | 0.54 | **1.59** | **− 0.73** | | |
| Level of significance for IPO −/IPO + differences | | p > 0.1 (not significant) | **p < 0.05** | **p < 0.05** | | |

(1) Number and percentage of ENSO events and ENSO neutral years; (2) the mean duration of ENSO events; (3) the month range in which the indices used to classify ENSO events are above the one standard deviation threshold; (4) the ENSO event SSTa magnitude in the eastern Pacific (10° N–10° S, 120°–90° W); (5) the ENSO event SSTa magnitude in the central Pacific (10° N–10° S, 180°–150° W); (6) the ENSO event SSTa magnitude in the North Pacific (35°–45° N, 180°–150° W); (7) the difference between central and North Pacific SSTa as an indicator of SSTa pattern differences. In (2), (4)–(7) it is indicated if the respective ENSO characteristics differ significantly between IPO − and IPO + phases. Below each metric, the significance level in the differences between IPO − and IPO + phases is indicated using a two-sample t-test. The significance levels shown are p < 0.1 (italic) and p < 0.05 (bold)

#### 3.2.1 CP El Niño

During both IPO + and IPO − phases, CP El Niño events are associated with significant positive SSTa in the central Pacific, stretching north-eastwards towards North America (Fig. 2a, b). The positive equatorial SSTa extent is quite similar in both IPO phases, and the differences between the CP El Niño patterns in the IPO phases are not statistically significant at the 5% level (Fig. 2c). The main difference lies in an area of cool SSTa that in IPO + phases straddles the warm equatorial SSTa in the subtropical region and Indonesian Throughflow region including north of Australia. This area of cool SSTa is typically associated with CP El Niño events in summer (Ashok et al. 2007), but is absent in IPO − phases (Fig. 2a, b).

The magnitude of positive equatorial central Pacific SSTa is generally similar in both IPO phases and all three seasons: SON, DJF and MAM + 1 (solid blue and red lines in Fig. 3a–c). The mean SSTa averaged over the central Pacific (180°–150° W) in DJF is + 0.67 °C during IPO − phases and + 0.55 °C during IPO + phases (Table 1). When the event peaks in DJF, the SSTa have a larger range in IPO − phases than they do in IPO + phases, with the highest and lowest central Pacific SSTa recorded in IPO − phases (Fig. 3b, blue shading).

#### 3.2.2 EP El Niño

During EP El Niño events in IPO − phases, statistically significant positive SSTa are equatorially confined between 10° N–10° S in the central to eastern Pacific (18-month average, Fig. 2d). In contrast, a much broader meridional SSTa structure and significantly stronger positive SSTa is evident in IPO + phases (Fig. 2e). Additionally, significant negative SSTa are present in the North Pacific, accompanied by significant warm anomalies along the north American west coast and warm anomalies in the Indian Ocean (Fig. 2e). This 'Indian Ocean Basin-wide warming' is a

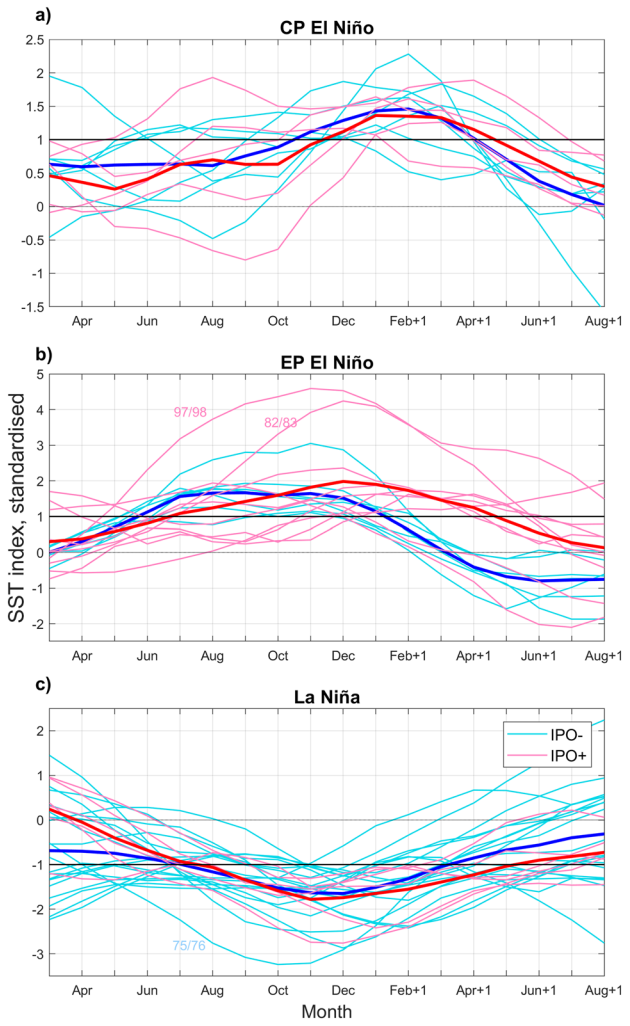


**Fig. 1** Duration and timing of ENSO events during IPO phases (1924–2015). Evolution of **a** CP El Niño, **b** EP El Niño and **c** La Niña events between March prior to and August after the peak of the ENSO event, separated by IPO phase. Light blue (pink) lines indicate all events that occurred in IPO − (IPO+) phases and the solid blue (red) line shows their average. The solid black line indicates the threshold (±one standard deviation) that needs to be exceeded to define an ENSO event

well-known response to EP El Niño during austral summer (Taschetto et al. 2011). Both features are absent in the EP El Niño composite during IPO − phases (Fig. 2d). Statistically significant differences between the EP El Niño/IPO − and EP El Niño/IPO + SSTa can be found in the North, central and eastern Pacific as well as in the Indian Ocean (Fig. 2f). The absence of the Indian Ocean Basin-wide warming during EP El Niño in IPO- phases has been noted previously by Liu et al. (2021), though only for the austral winter (July to September) following the peak of the ENSO event. Liu et al. (2021) linked the absence of the Indian Ocean Basin-wide warming in IPO − phases to EP El Niño events dissipating earlier and hence not lasting as long in IPO − compared to IPO + phases.

In summer (DJF) and autumn (MAM + 1), the mean equatorial Pacific SSTa are significantly stronger in IPO + phases than in IPO − phases throughout the central and eastern Pacific (solid blue and red lines in Fig. 3e, f). For example, in DJF the mean eastern Pacific (120° W–90° W) SSTa is 1.12 °C compared to 0.62 °C during IPO − phases (Table 1). There is also a much larger spread in eastern Pacific SSTa in IPO + phases, with SSTa maxima exceeding 2 °C in the Niño 1 + 2 region. This reflects the tendency for extreme EP El Niño events to occur more often during IPO + than during IPO- phases (Fig. 3d–f). A significant difference in mean SSTa during MAM + 1 (Fig. 3f) is consistent with EP El Niño events remaining active for longer during IPO + phases compared to IPO − phases.

### 3.2.3 La Niña

La Niña events during IPO − phases are characterised by significant negative SSTa that stretch throughout the central and eastern equatorial Pacific and into the Northern and Southern Hemispheres over a broad area, along with basin-wide cooling in the Indian Ocean (Fig. 2g). Significant positive SSTa are observed in the North Pacific and south of the Niño regions, in the approximate location of the South Pacific Convergence Zone (SPCZ; Fig. 2g). In IPO + phases, the La Niña SSTa pattern is different in three main aspects. First, the cool SSTa are confined to within 15° N–15° S, and do not extend beyond the central Pacific. Second, strongly positive SSTa are evident off Western Australia, which resemble a Ningaloo Niño pattern. Third, weakly cool SSTa are seen in the North Pacific (Fig. 2h). These differences are statistically significant in the Pacific off-equatorial 'wing' region north and south of the equator, in the North Pacific and Indian Ocean (Fig. 2i).

During SON and DJF and in IPO + phases, negative SSTa along the equatorial Pacific have the greatest magnitudes in the central Pacific and weaken towards the east. During the same seasons in IPO − phases, the negative equatorial SSTa extend into the far eastern Pacific. By MAM + 1, these cool SSTa weaken in both IPO phases (Fig. 3g–i). While the central Pacific SSTa magnitude does not differ significantly between IPO + and IPO − phases, significant differences are seen in the eastern Pacific during SON and DJF (Fig. 3g, h) and in the western Pacific warm pool region in SON and MAM + 1 (Fig. 3g, i). We further observe a tendency for the strongest La Niña events to occur during IPO − phases as indicated by the minimum SSTa of − 0.71 °C in the equatorial Pacific compared to − 0.38 °C in IPO + phases (Fig. 3g–i, Table 1).

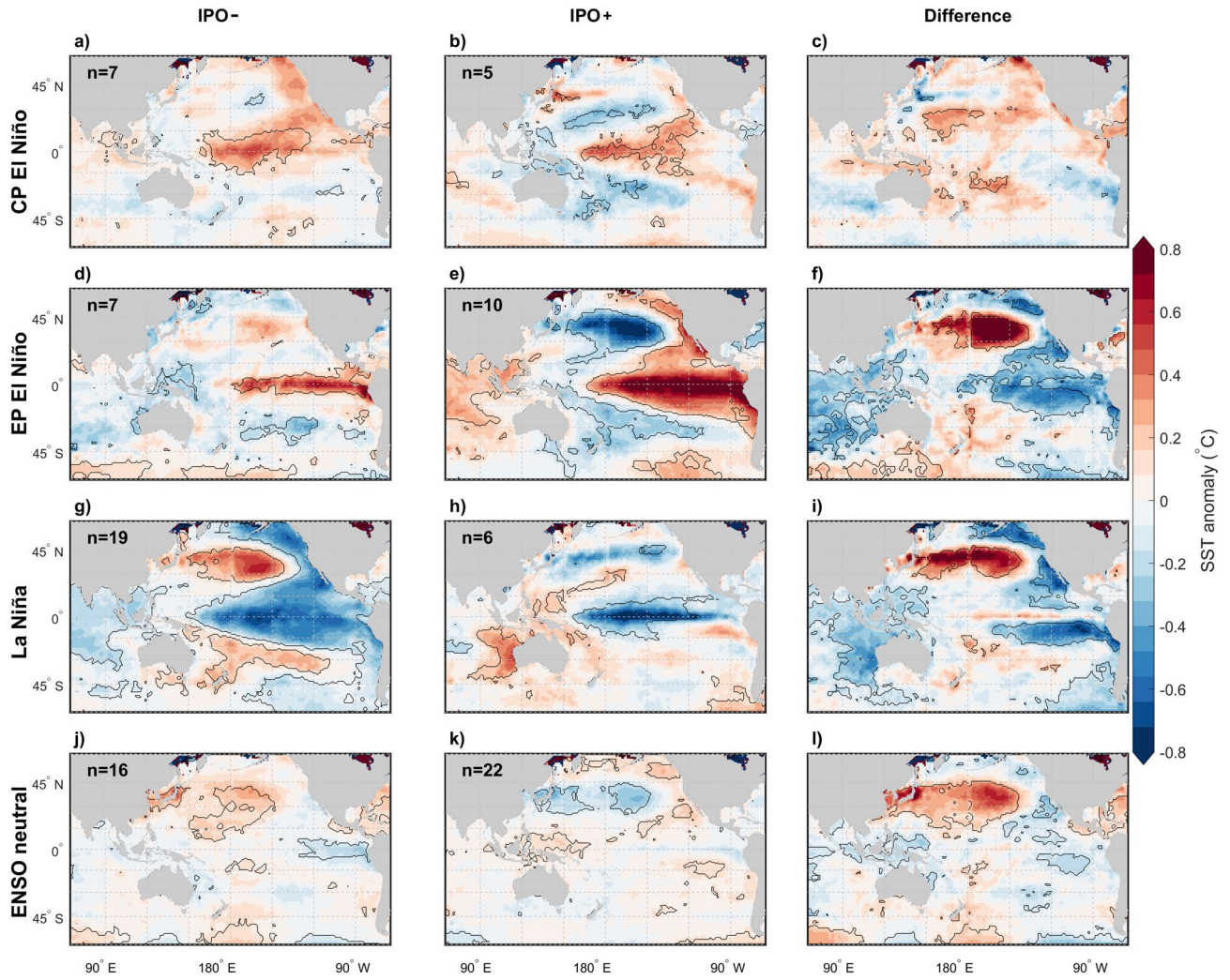


**Fig. 2** SSTa composites associated with ENSO and ENSO neutral years during IPO − and IPO + phases (between 1924 and 2015), including the difference between the IPO phases. Composite SSTa during **a–c** CP El Niño events, **d–f** CP El Niño events, **g–i** La Niña events and **j–l** ENSO neutral years are averaged over 18 months around the peak of the event (from March prior to the peak in austral summer to August after the peak of the event (M to A + 1). Significant anomalies (black contours; $p < 0.05$) are computed using a Monte Carlo method (see Sect. 2 for details). The composites are divided into (left) IPO −, (middle) IPO + phases, and (right) SSTa difference between IPO − and IPO + phases (IPO–IPO + SSTa) for each ENSO event type. In the difference maps, black contours indicate significant differences between both data distributions, determined through a two-sample t-test

#### 3.2.4 ENSO neutral

To provide a complete picture of all years that make up each IPO phase, SSTa composites of ENSO neutral years are discussed here (Fig. 2j, k). When ENSO is neutral during an IPO − phase, significant positive SSTa are seen in the North Pacific. The opposite is true when the IPO is positive and ENSO is neutral, meaning the IPO − and IPO + differences for ENSO neutral years are significant in the North Pacific (Fig. 2l). In both IPO + and IPO − phases, central Pacific SSTa are generally not significant at the 5% level during ENSO neutral years, and as such, differences between ENSO neutral SSTa in IPO − and IPO + phases in the central Pacific are small and insignificant (Fig. 2j–l).

### 3.3 SST variability associated with the IPO

In this subsection we investigate decadal SST characteristics that are directly related to the IPO during DJF, when the tropical Pacific variability is usually the strongest. This is done to identify the mean SSTa and variability patterns between IPO + and IPO − phases.

A IPO + (IPO −) phase is associated with warm (cool) SSTa in the central to eastern Pacific, which extend into the subtropical regions in both hemispheres. A 'blob' of

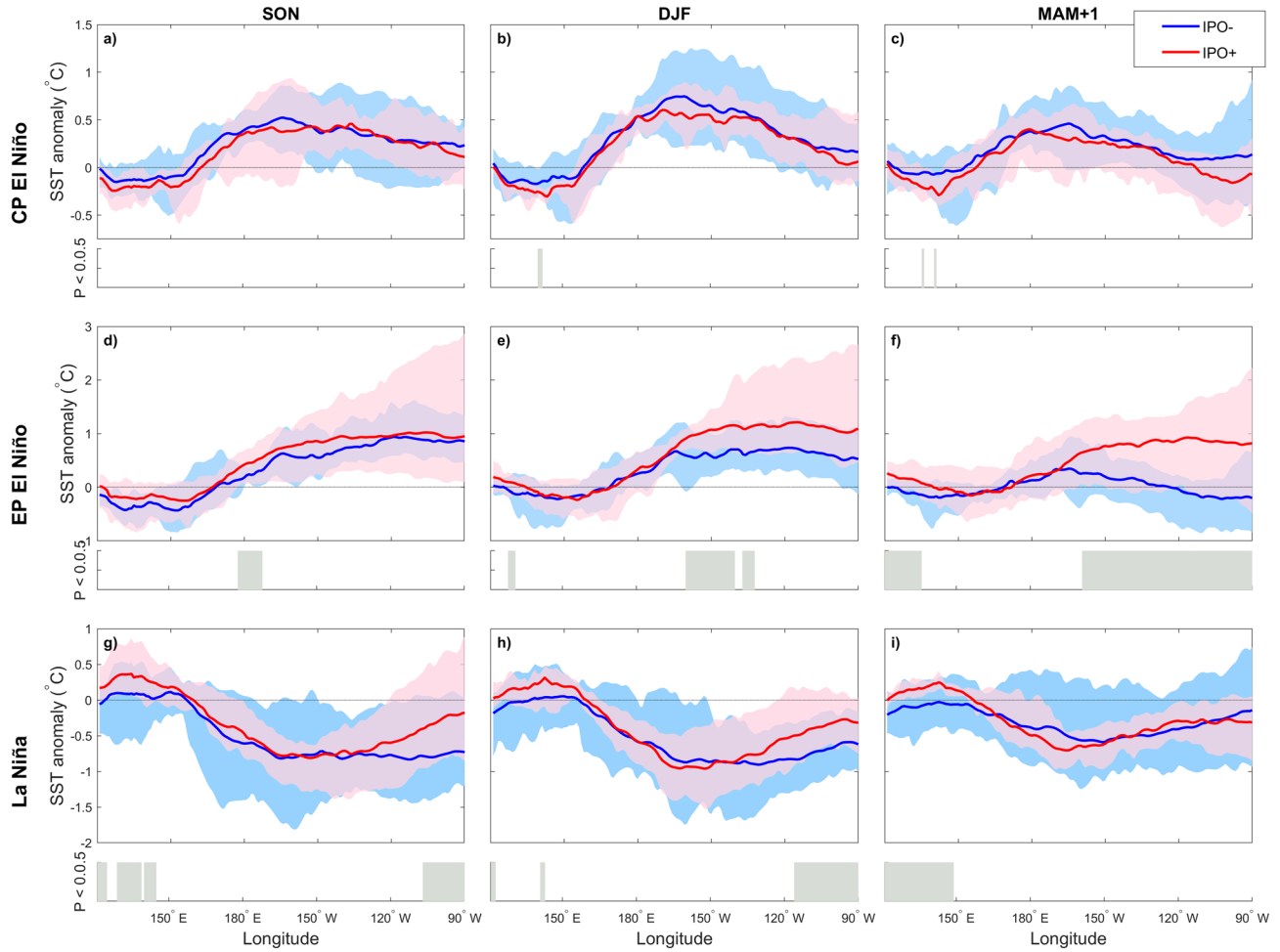


**Fig. 3** SSTa profiles for ENSO events during IPO phases. Shown are SSTa profiles averaged over the equatorial Pacific (10° N to 10° S) for ENSO events in IPO − and IPO + phases between 1924 and 2015. Seasonal averages are calculated over (left) SON; (middle) DJF and (right) MAM for **a**–**c** CP El Niño, **d**–**f** EP El Niño and **g**–**i** La Niña events. Dark blue lines and light blue shading indicate the mean SSTa and SSTa range of all respective ENSO events during IPO − phases, respectively. Red lines and pink shading indicate the mean and range for IPO + phases. Note that the vertical axes differ between CP El Niño, EP El Niño and La Niña. Statistical significance (p-value $<0.05$) in the difference between SSTa in IPO − and IPO + phases is shown with a grey bar below each SSTa profile

opposite sign SSTa is located in the North Pacific, displaying cool SSTa during IPO + and warm SSTa in IPO − phases (Fig. 4a, c). This mean IPO pattern is consistent with what has been shown in previous studies (e.g. Power et al. 1999; Henley 2017). To determine if the mean SSTa patterns during IPO − and IPO + phases are asymmetric, we sum the anomalies. The asymmetry of both SSTa patterns is weak and not significant (Fig. 4e). Therefore, the difference in ENSO event SSTa patterns between IPO − and IPO + phases (e.g., broader equatorial SSTa during one and equatorially confined SSTa in the other IPO phase for both La Niña and EP El Niño) cannot simply be explained by the differences in mean IPO (background) SSTa. Additional factors need to be considered.

The spatial distribution of the interannual standard deviation is also similar in IPO − and IPO + phases (Fig. 4b, d). While the central Pacific has the highest standard deviation of SSTa, this region of high standard deviation extends further into the eastern Pacific in IPO + compared to IPO- phases; this difference in the eastern Pacific is significant (Fig. 4f). A high standard deviation is also observed in the North Pacific during both IPO phases. In addition, in IPO − phases, the Tasman Sea off southeast Australia shows a higher standard deviation compared to the oceans surrounding Australia. This region of high variability shifts east of New Zealand in IPO + phases (Fig. 4b,d).

Next, we evaluate the Relative Frequency Distributions of the detrended TPI for each individual IPO phase. The highest positive TPI is observed in the most recent IPO + phase (1977–1998), while the strongest negative TPI is observed during the most recent IPO − phase (1999–2014; Fig. 4g). A similar tendency can be seen for the Niño 3.4

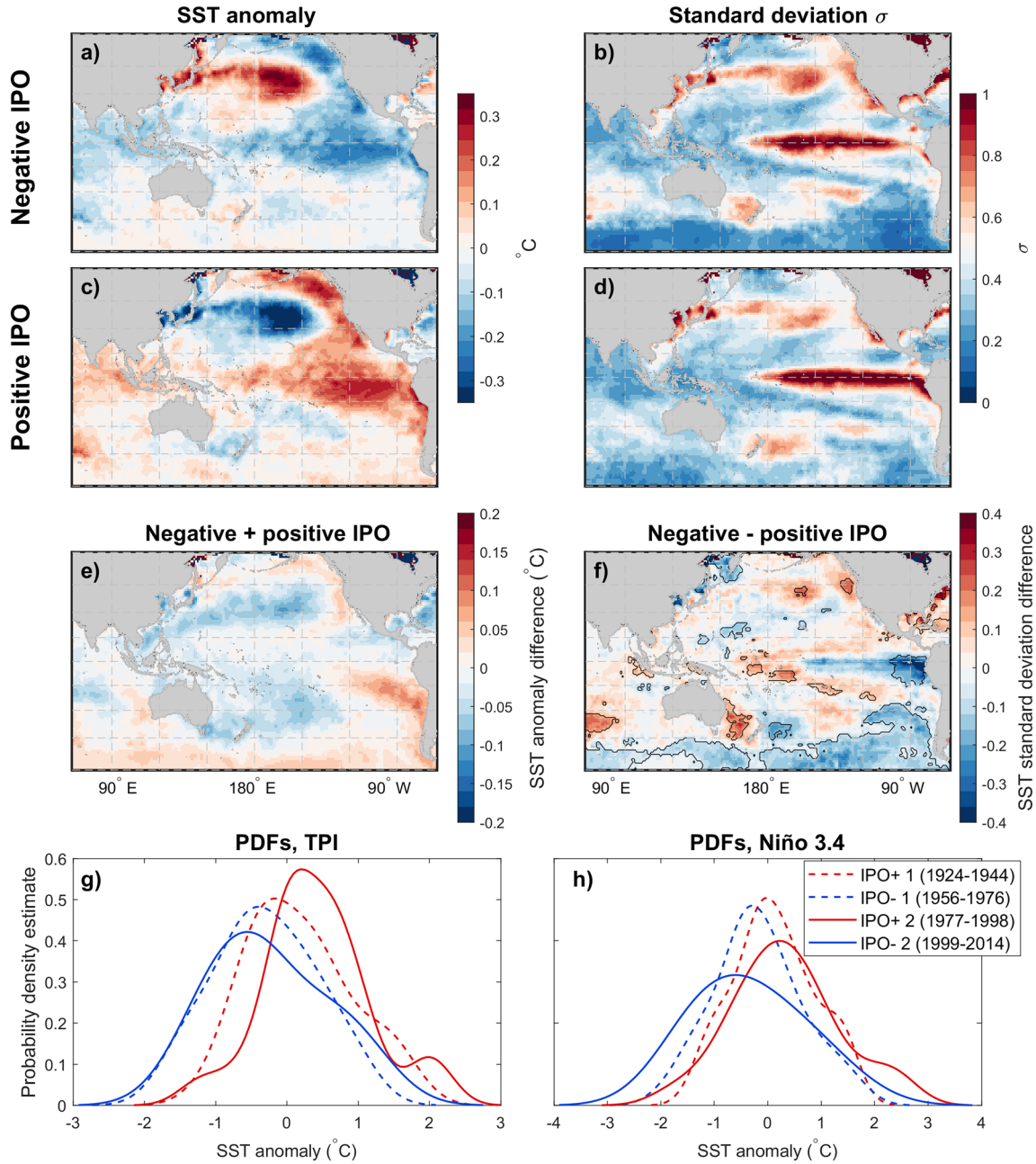


**Fig. 4** SSTa during IPO phases (1924–2015). Mean SSTa patterns (**a**, **c**) and interannual standard deviation σ (**b**, **d**) during IPO − (**a**, **b**) and IPO + (**c**, **d**) phases in DJF. The sum of both SSTa patterns is displayed in panel **e** to examine the asymmetry. The difference between both standard deviations is included in **f**. Probability distributions for the TPI and the Niño 3.4 index, separated into each individual IPO phase, are shown in **g** and **h**

index (Fig. 4h). It appears that increased SST variability in the tropical and extratropical Pacific has occurred in the most recent decades. As to why this is the case, this needs to be further tested in a future study, but it is consistent with a late twentieth century increase in ENSO variability (Cai et al. 2023).

### 3.4 EOFs and corresponding timeseries

Here, we examine the first EOF mode of the large scale interannual and decadal SSTa in DJF with a focus on the Pacific Ocean (Fig. 5a, b) as well as their associated principal components (PCs; Fig. 5c). If $H_0$ is true, both interannual

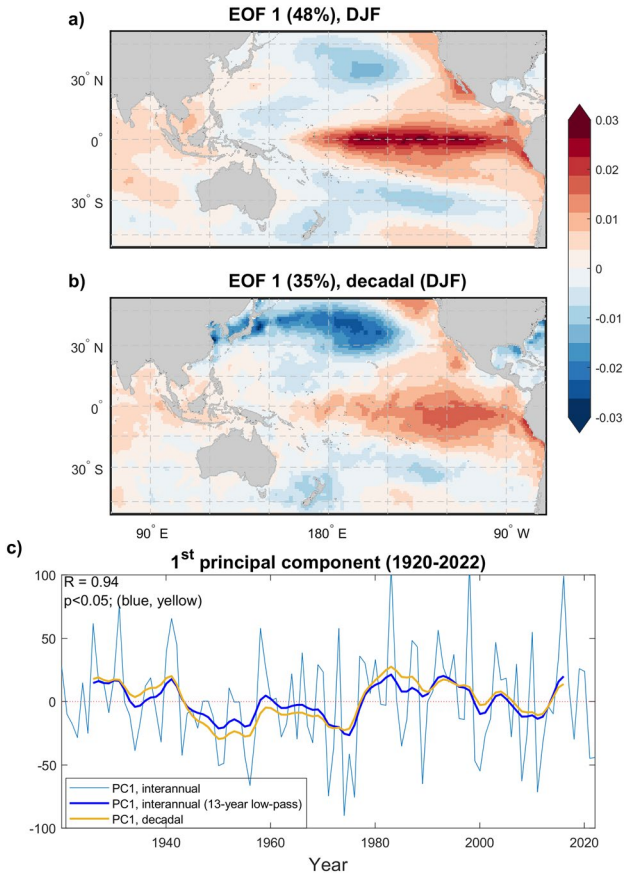


**Fig. 5** The dominant EOF pattern and associated timeseries of large-scale interannual and decadal SSTa (1920–2022). The first EOF of SSTa in austral summer on interannual (**a**) and decadal (**b**) timescales. For decadal timescales a 13-year low-pass filter is applied prior to the analysis. The associated PCs are shown in **c**. The first PC for an interannual timescale is depicted unfiltered (light blue line), as well as with 13-year low-pass filter applied (thick blue line), and the first decadal PC is included as well (yellow line). The correlation coefficient R between both filtered timeseries is included in **c**

and decadal EOFs should be very similar. Comparing both will help to determine this.

Given the null hypothesis ($H_0$) introduced earlier, we are particularly interested in two aspects. First, what are the similarities and differences between the interannual and decadal EOFs (i.e., spatial patterns)? Second, is the decadal variability in the interannual PC (i.e., time series) similar to the variability evident in the decadal PC? A strong similarity is consistent with $H_0$, while a robust difference might indicate limitations in the applicability of $H_0$. Power and Colman (2006), for example, found that decadal variability in the leading PC of interannual Pacific variability in their Coupled General Circulation Model was strongly correlated ($R = 0.98$).

The first EOF of interannual SSTa shows the classical ENSO pattern (Fig. 5a), with the strongest loading centred in the central to eastern equatorial Pacific that decreases meridionally. The first EOF of decadal SST, which represents the IPO, is characterised by a V-shaped loading around the central to eastern equatorial Pacific that extends into the subtropics in both hemispheres. The peak loadings of the decadal EOF are located in the eastern Pacific, approximately between 130° W and 90° W. A strong loading of opposite sign is evident in the decadal EOF in the North Pacific from 150° E to 150° W. The decadal EOF differs from the interannual pattern, showing a broader region of increased equatorial Pacific loading and a much stronger signal in the North Pacific (Fig. 5b), as previously noted by Henley (2017). The meridional extensions are also a distinct feature for decadal timescales and the extensions have previously been described as 'wings' (Power and Colman 2006). Another difference, which stands out by comparing interannual (Fig. 2) and decadal patterns (Figs. 4, 5) is the further westward extension of the decadal SSTa in the tropical Pacific, which reaches into the western warm pool region.

When a 13-year low-pass filter is applied (thick blue line, Fig. 5c), the resulting filtered timeseries reveals a strong resemblance to the first decadal PC (yellow line). Both filtered timeseries are significantly correlated ($R = 0.94$, $p < 0.05$), consistent with $H_0$. The difference in the EOF spatial structures, particularly the 'wing' structure and the enhanced extratropical variability in the North Pacific that is only detected in the decadal EOF, might suggest some distinct differences between the interannual and decadal modes of variability. This possibility is explored further in the following section.

### 3.5 Comparison of ENSO event and IPO pattern

In this section, we examine the similarities and differences between the SSTa patterns representing decadal IPO and interannual ENSO events. We again compare and contrast SSTa composites for La Niña, CP El Niño and EP El Niño during IPO + with those during IPO − phases, as shown in Fig. 2, with the IPO SSTa for both positive (Fig. 4a) and negative (Fig. 4c) phases.

The broad tropical negative SSTa and North Pacific warm 'blob' found in the IPO − La Niña composite (Fig. 2g) shows a strong resemblance to the IPO − pattern (Fig. 4a). The correlation coefficient between the IPO − La Niña pattern and the IPO − pattern using the whole map area depicted in Fig. 2 and Fig. 4, is statistically significant ($R = 0.81$, $p < 0.05$). In IPO + phases, EP El Niño events show a slightly narrower positive SSTa pattern centred on the equator than the mean IPO + pattern, with a 'blob' of negative SSTa in the North Pacific (Fig. 2e). There is a strong resemblance between the EP El Niño SSTa pattern (Fig. 2e) and the IPO + pattern ($R = 0.9$, $p < 0.05$).

The ENSO event composites considered so far are obtained using SSTa averaged over an 18-month period,

from March to August the following year, a period which includes the initiation, growth, peak, decay and termination of each event. It is also of interest to compare IPO patterns with ENSO event composites over shorter periods to see if the results change and the ENSO event patterns become more IPO-like (e.g., a broader SSTa pattern around the equator) when increasing the timeframe that is included. In Supplementary Fig. 1, we show SSTa composites for ENSO events as seasonal averages using the same 18-month period (March to August in following year). The seasonal averages, compared to the 18-month averages in Fig. 2, reveal that the SSTa patterns of both EP El Niño in IPO + and La Niña events in IPO − phases become broader around the equatorial Pacific and stretch further into both hemispheres when the timeframe increases from seasonal to 18-month averages and the SSTa patterns better resemble the IPO patterns.

The same positive (negative) North Pacific SSTa evident in the mean IPO − (IPO +) SSTa is also visible in ENSO neutral years, during EP El Niño and La Niña events (Fig. 2j, k). It is only during CP El Niño events that the North Pacific SSTa are not consistent with the mean IPO SSTa pattern. CP El Niño events are associated with weakly negative SSTa in the North Pacific in both IPO + and IPO − phases, and hence show little difference between the IPO phases.

### 3.6 Interannual and decadal SSTa correlations with Niño 3.4

As noted above, there is a difference in the meridional extent of the 'wing' pattern between the first EOF of interannual and decadal SSTa patterns (Fig. 5). Here we examine if this difference is robust and why these differences might arise. We begin by examining the correlation coefficient between the Niño 3.4 index and off-equatorial SSTa on interannual and decadal timescales. This same approach was used by Power and Colman (2006) to better understand the origin of multi-year and decadal variability in the off-equatorial Pacific in their climate model.

Here, we include all months of the year with the resultant correlation map for interannual and interdecadal SSTa shown in Fig. 6a, b. The maps show that the magnitude of the correlation coefficients between Niño 3.4 SSTa and off-equatorial Pacific SSTa around 15 °S to 30 °S and °N are larger on interdecadal timescales (13-year low-pass filter applied to both) than they are on interannual timescales [see e.g. "NH" (23.5° N, 145.5° W) and "SH" (21.5° S, 150.5° W) in Fig. 6c, both are in the wing regions referred to above]. This is consistent with the modelled results obtained by Power and Colman (2006). Please note that detrending did not affect the interpretation of these results, with similar SSTa patterns arising when the data are not detrended.

Two other differences between the interdecadal and interannual patterns are evident. First, the interdecadal scale

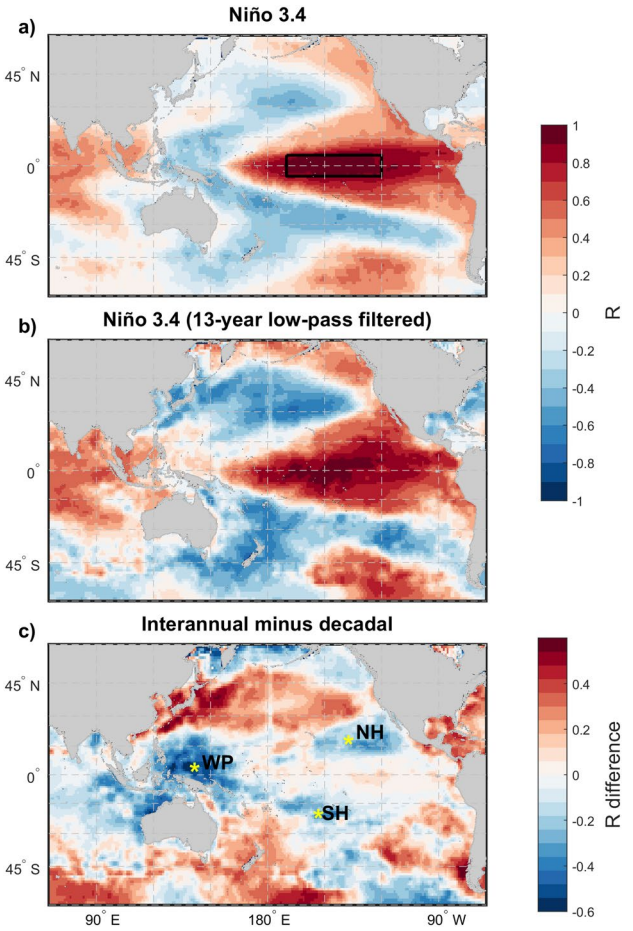


**Fig. 6** Correlation coefficient (R) between the Niño 3.4 index and grid point SSTa between 1920 and 2022. Correlations shown for **a** interannual; location of Niño 3.4 region shown by black box; and **b** decadal (13-year low-pass filtered) timescales, as well as **c** the difference between both correlation coefficients (panel **a** minus panel **b**). Three locations are marked (yellow marker) in regions where the difference between interannual and decadal correlation coefficients was particularly strong: one in the Northern Hemisphere (NH), one in the Western Pacific (WP) and one in the Southern Hemisphere (SH)

positive correlations around the equatorial Pacific extend much further into the western Pacific and into the Indian Ocean compared to the interannual correlation patterns [see Fig. 6c, yellow asterisk marked "WP" (3.5° N, 140.5° E)]. Second, the interdecadal patterns show a large area with negative correlation coefficients in the North Pacific, stretching from approximately 120° E to 130° W. These correlation coefficients (Fig. 6b) are larger in magnitude than their interannual counterparts (Fig. 6a).

An evaluation of specific grid points in the 'wing' areas with particularly strong differences in the correlation coefficients (NH, SH and WP grid points) and their lag/lead correlations with Niño 3.4 is conducted in Supplementary Materials 2. The 13-year low-pass-filtered SSTa at all three locations indicate the tendency of the maximum correlation

with Niño 3.4 leading the SSTa by one to 6 years (lags > 0). The results indicate that both raw and decadally filtered SSTa in the 'wing' region to the north, west and south of the Niño 3.4 region are, to a varying degree, a delayed response to low-frequency Niño 3.4 variability (Supplementary Fig. 2). Using the lagged relationship, the filtered Niño 3.4 index accounts for between 24 to 40% of the low-frequency SSTa variability in these three regions (NH: $R^2 = 0.3$; WP: $R^2 = 0.38$; SH: $R^2 = 0.24$). Due to the relatively small correlations, it is likely that other factors in addition to Niño 3.4 need to be accounted for when analysing the SST variability in these 'wing' regions and therefore the IPO pattern.

### 3.7 Reconstructing the IPO from ENSO event frequency and duration

Previous research (Power et al. 2021) showed that indices of decadal variability in the Pacific could be mimicked to an extent by tracking decadal differences in the relative frequency of El Niño and La Niña events. Here we extend this work to determine the extent to which an IPO index can be reproduced using decadal variability of both ENSO event frequency and ENSO event duration. We determine which event types are most influential in driving the IPO index under $H_0$.

We begin by using a simple statistic that only includes information on the relative frequency of ENSO events [n(El Niño) − n(La Niña) divided into 5-year blocks and using a running sum; after Power and Smith (2007) and Power et al. (2021)]. The resulting time series has a correlation coefficient with the TPI of 0.6, which is statistically significant at the 5% level (Fig. 7a). Interestingly, when we repeat the analysis, but use the frequency of only El Niño events, the correlation coefficient drops to 0.23 and is not statistically significant. Using − n(La Niña), i.e., minus one times the frequency of La Niña events only, the correlation coefficient increases in magnitude to 0.61 (statistically significant). Therefore, decadal variability in the relative frequency of El Niño and La Niña events, alone, with no additional information on the magnitude, duration or other characteristics of the events, explains approximately 36% of the decadal variability in the TPI.

We next attempt to reconstruct the TPI by also including information on the long-term average magnitude of Niño 3.4 anomalies for each type of ENSO event (EP and CP El Niño, La Niña). We generate an artificial timeseries by inserting the respective mean Niño 3.4 SSTa into the years in which an ENSO event occurred, and a zero for ENSO neutral years. This new timeseries is then smoothed with a 13-year low-pass filter and plotted against the smoothed

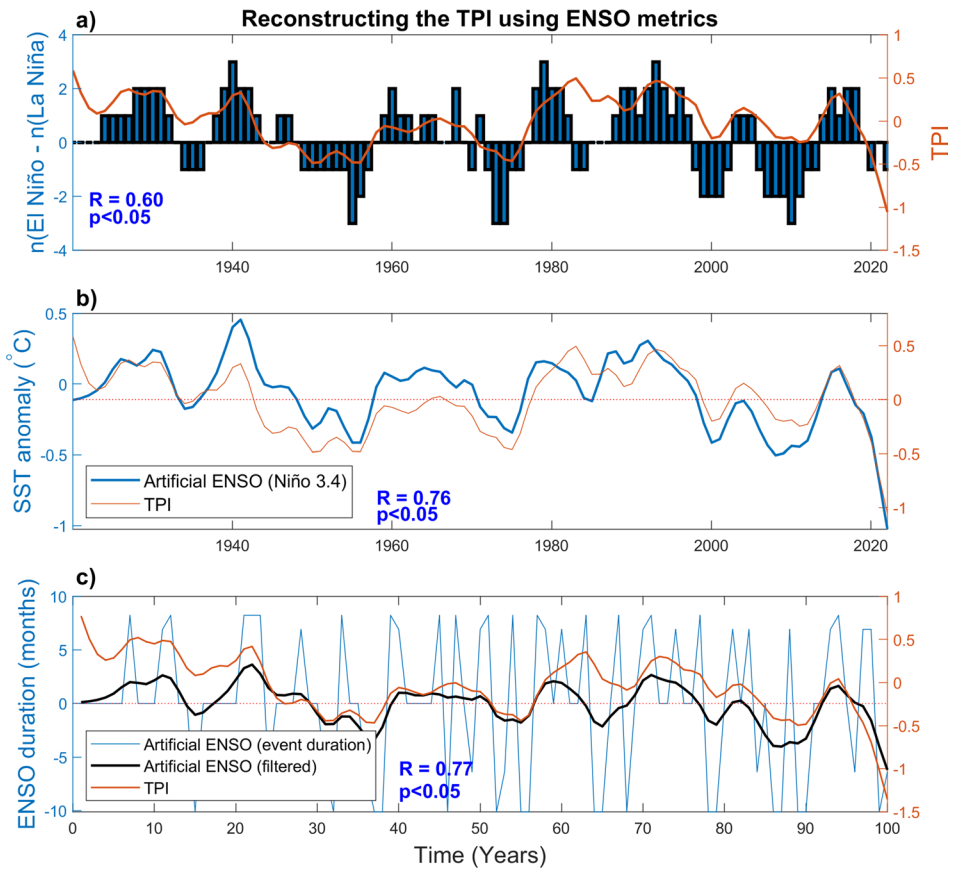


**Fig. 7** Timeseries plots of the TPI and three artificially generated ENSO metrics: **a** Timeseries of the relative frequency of El Niño and La Niña events (number of El Niño − number of La Niña events using 5-year running sum) and the 13-year low-pass filtered TPI; **b** artificial timeseries of mean Niño 3.4 values inserted in each ENSO year and the TPI, both low-pass filtered; **c** timeseries generated with the number of months for the mean duration of each ENSO event type, the same low-pass filtered timeseries and the TPI, also low-pass filtered. Note that for El Niño, the duration in months is inserted as a positive value while for La Niña, the duration is inserted as a negative value. The time series does not exactly match up with **a** and **b** due to events with a duration longer than 12 months, for which the TPI value in the second year was removed to adjust the length of both timeseries. Statistical significance is assessed using block bootstrapping (see Sect. 2)

TPI in Fig. 7b. The resulting timeseries is again similar to the TPI, and the correlation coefficient is again statistically significant ($R = 0.76$, $p < 0.05$). This suggests that information on the differences between the long-term average SSTa during CP El Niño, EP El Niño and La Niña events marginally improves the reconstruction of the TPI compared to only using ENSO event frequency.

Next, we determine the extent to which the TPI can be reproduced using information on both the duration and relative frequency of ENSO events. The method is similar as described in the previous paragraph, only that the mean duration (in months) for each ENSO event type is inserted in the ENSO years and a '0' in ENSO neutral years. The mean duration for La Niña is multiplied by − 1 for consistency. The correlation coefficient between the resulting artificial timeseries and the TPI is 0.77 and is again statistically significant ($p < 0.05$; Fig. 7c). This indicates that the stronger the positive TPI (IPO +) is, the longer El Niño events lasted. Similarly, the stronger the negative TPI (IPO −) is, the longer La Niña events lasted. Due to the lower number of ENSO events in IPO + phases and therefore more zeros in the time series the frequency of ENSO events plays an indirect role in generating this statistic. We conclude that duration does increase the correlation coefficient compared to only using the relative frequency of ENSO events, by a similar magnitude to using the mean event Niño 3.4 SSTa.

## 4 Discussion

In this paper, we examined statistical relationships between ENSO, ENSO diversity and the IPO. This work was motivated by the knowledge gap in the mechanisms that cause decadal variability in the Pacific Ocean as noted in previous studies, including the role of ENSO (e.g. Power et al. 2021). Subsequently, we investigated the decadal variability in ENSO characteristics, the IPO itself and their interconnection. We tested the null hypothesis ($H_0$) that the IPO is a statistical residual of decadal variability in ENSO activity (Power and Colman 2006) and the more sophisticated alternative null hypothesis that some of the IPO SSTa variability arises as an oceanic response to preceding decadal variability in ENSO (Power and Colman 2006; Power et al. 2021). We focussed on statistical relationships evident in gridded SSTa data from 1920 to 2022, and from 1924 to 2015 for IPO − and IPO + specific results. This second null hypothesis is referred to as $G_{0.}$

### 4.1 Results consistent with $H_0$

One of the main reasons for conducting this study was to determine whether the statistical relationships between IPO and ENSO are consistent with the null hypothesis, $H_0$, in which all IPO variability is a statistical artefact of decadal variability in ENSO activity, and for which predictability beyond 1 year is absent (Power et al. 2006; Power and Colman 2006).

Key findings are listed in Table 2 as 'Summary points'. Summary points 1, 6, 8, 9, 12 and 13 (Table 2) are, to a degree, consistent with $H_0$. Three times as many La Niña events occur in IPO − compared to IPO + phases, while the increase in frequency of EP El Niño events in IPO + phases is only small (Table 1; summary point 1 in Table 2). Therefore, the increased occurrence of La Niña in IPO − phases and the reduced number of La Niña events in IPO + phase are what mainly leads to the frequency of ENSO events being able to explain more than a third of the low-frequency variability of the TPI (Fig. 7; summary point 12 in Table 2). This is in good agreement with Power and Colman (2006) who consider that the IPO is partly a representation of times when La Niña events occur more often (IPO −) versus times when El Niño events dominate. The event magnitude and duration also play a role (summary point 8, 9, 13 in Table 2), as by including either of them in the reconstruction of the TPI, up to 59% of the IPO's variability can be explained.

In a more recent study, Power et al. (2021) find a strong resemblance between the relative frequency of ENSO events and their tropical decadal variability index. We show here that the first decadal PC and the first interannual PC (with a low-pass filter applied) are almost identical ($R = 0.94$, Fig. 5; summary point 6 in Table 2). This update supports previous analysis presented by Power et al. (2006). The striking similarity of the interannual and decadal modes of variability, which represent ENSO and the IPO respectively, suggests that they are closely connected. Therefore, the differences in the relative frequency of ENSO events, as well as the relationship between the artificially generated ENSO timeseries and the TPI, support the $H_0$. Further to this, the $H_0$ is consistent with the similarity of the interannual and decadal PCs of Pacific SSTa.

While consistent with $H_0$, an alternative interpretation of the relationship between the relative frequency of ENSO events and the IPO can also be seen the other way around—as ENSO responding to changes in the background state within, or outside the tropical region (Okumura et al. 2017). It could further be argued that low-frequency variations in the interannual PC simply describes the tropical signature of the IPO.

### 4.2 Results supporting $G_0$

We next discuss results that do not support $H_0$, but may be explained by a slightly more complex hypothesis. A more sophisticated null hypothesis ($G_0$) posits that some of the IPO variability is a lagged response to preceding surface

**Table 2** Summary of the important findings from the Sect. 3

| Summary points |
|---|
| (1) La Niña events occurred about three times more often in IPO − phases (39% of all IPO − years were La Niña years) than in IPO + phases (14% of all years were La Niña years) while there was little decadal difference in the frequency of El Niño events (Table 1) |
| (2) During EP El Niño and La Niña events, the SSTa patterns differed significantly between IPO − and IPO + phases in the Pacific 'wing' off-equatorial region, as well as in the North Pacific and Indian Ocean (Fig. 2f, i) |
| (3) Statistically significant differences in North Pacific SSTa between IPO − and IPO + phases were observed during ENSO neutral years (Fig. 2l) |
| (4) The IPO − and IPO + mean SSTa patterns are similar and symmetric. The standard deviation differs in the eastern Pacific, where it is stronger during IPO + compared to IPO − phases (Fig. 4) |
| (5) The decadal EOF differs from the interannual one in a broader structure in the off-equatorial 'wing' region and stronger loadings in the North Pacific (Fig. 5a, b) |
| (6) The filtered interannual and the interdecadal PCs of SSTa are very similar (Fig. 5c) |
| (7) A strong SSTa dipole pattern is observed between the North and equatorial Pacific during EP El Niño in IPO + phases and La Niña in IPO − phases, but not in the respective opposite IPO case (EP El Niño in IPO − and La Niña in IPO + phases). This reflects significant SSTa differences in the Pacific Ocean during these ENSO events due to the IPO phase (Fig. 2d–i) |
| (8) During EP El Niño, the warm equatorial SSTa were significantly stronger in IPO + compared to IPO− phases (Fig. 3e, f). This was the case in DJF in the central Pacific and in both central to eastern Pacific in the following MAM (+ 1) and is consistent with the warm IPO background state |
| (9) During La Niña, the cool SSTa in the eastern Pacific were significantly stronger in IPO − compared to IPO + phases during the developing spring (SON) and peak of the event (DJF; Fig. 3g, h). This is consistent with the cool IPO background state |
| (10) The 'wing' region is where the correlation coefficient between Niño 3.4 and grid point SSTa differed the most between interannual and interdecadal timescales (Fig. 6) |
| (11) At three specific locations in the 'wing' region, the SSTa have a lagged relationship with the low-pass filtered Niño 3.4 index leading. This applies to both raw and low-frequency variability in SSTa at these locations (Suppl. Materials 2) |
| (12) The frequency of all ENSO events was able to explain about a third (36%) of the low-frequency variability of the TPI (Fig. 7a). The frequency of El Niño plays a negligible role in this statistic, which is dominated by the strong relationship between the TPI and the frequency of La Niña events |
| (13) The average magnitude and duration of ENSO events do marginally increase the relationship with the TPI compared to using the relative frequency of the events only ($R^2 = 0.59$; Fig. 7b, c) |

fluxes of heat or momentum and that the fluxes are at least partially driven by ENSO (Power and Colman 2006). This very behaviour was evident in a coupled atmosphere–ocean model in off-equatorial Pacific regions (Power and Colman 2006). Important properties of this type of variability are that it should lag ENSO indices like Niño 3.4, and that it should be more coherent with Niño 3.4 and other ENSO indices on multi-year through to decadal timescales (Power and Colman 2006). For IPO SSTa that are driven by surface heat fluxes that are fractionally ENSO driven, the resulting variability can be considered as an ENSO-modified form of Hasselmann-like variability. For this sort of variability, the correlation coefficients at zero lag tend to be higher on multiyear or longer timescales than they are on interannual timescales, and ENSO indices like Niño 3.4 SSTa variability (filtered and unfiltered) tends to lead the grid point SSTa variability (Power and Colman 2006) in time.

We found that these features were indeed evident in summary points 2, 5, 7, 10 and 11 (Table 2), consistent with $G_0$. It is well known that the ENSO SSTa develop around the equatorial Pacific, while the decadal IPO pattern is associated with a much broader 'wing' like area of SSTa, accompanied by opposite sign SSTa in the North Pacific. This is evident, for example, when comparing interannual and decadal EOFs (summary point 5 in Table 2), correlation coefficients (summary point 10 Table 2) as well as ENSO event composites with mean IPO SSTa. A strong correlation between the 18-month averaged SSTa pattern for the IPO − La Niña composite with the general IPO − SSTa, as well as the IPO + EP El Niño composite with the IPO + pattern is observed. This suggests a connection between the IPO pattern and ENSO as La Niña is related to the IPO − pattern and EP El Niño is connected to the IPO + pattern. However, these pattern correlations do not explain the causal pathway of this relationship. Power et al. (2021) show a good agreement between the tropical Pacific decadal variability pattern that resembles the IPO, and the 2-year average of El Niño. Expanding on this, here we show that the strong resemblance between ENSO and IPO patterns applies to both EP El Niño and the IPO + patterns, and La Niña and the IPO − patterns, and that CP El Niño events seem to have little connection to the IPO pattern. The significant differences between the meridional extent of the equatorial Pacific SSTa during these EP El Niño and La Niña events between IPO − and IPO + phases (Fig. 2f, I; summary point 7 in Table 2) is consistent with earlier research (Power and Colman 2006).

To dynamically link ENSO and the IPO, not only statistically, and determine which of them modify the other, oceanic processes need to be investigated. It is further suggested that when the development and demise of an ENSO event are included into the composites rather than focusing on the peak of the event in austral summer only, the equatorial SSTa push further into the off-equatorial regions, forming the broader IPO-like pattern (Vimont 2005; Power et al. 2021). In other words, taking the whole evolution of El Niño into account results in a broader SSTa pattern as opposed to focusing on the austral summer alone. We find that this is only true for certain ENSO cases: EP El Niño in IPO + and La Niña in IPO − phases, while no broadening occurs for their counterpart cases or CP El Niño events (Fig. 2; summary point 2 and 7 in Table 2). Therefore, possibly, the broad IPO SSTa could be a lagged version of the ENSO event type that dominates in the respective IPO phase. Vimont et al. (2001) and Power et al. (2021) have in fact shown that the decadal SST broadening can arise from the lagged relationship between tropical and extratropical SSTs. We explore this possibility in Supplementary Fig. 2 by evaluating lag correlations between the filtered Niño 3.4 index and SSTa in three locations in the 'wing' region, in which there was a particularly strong difference in correlation coefficients between interannual and decadal timescales (summary point 10 in Table 2). In all three locations, the NH, SH and WP, the correlation coefficient increases when the filtered Niño 3.4 index leads the SSTa in those areas. The results indicate that both raw and filtered SSTa in the 'wing' region are at least partly driven by the preceding low-frequency variability in the tropical Pacific (summary point 11 in Table 2). The fact that the equatorial SSTa leads the SSTa in the off-equatorial region where the IPO and ENSO patterns differ, adds further weight to the idea that SSTa in those regions are at least partially forced by ENSO rather than the other way around. These results are consistent with $G_0$.

The findings shown here expand on a previous model-based study by Power and Colman (2006) who also found a lag correlation between off-equatorial surface and subsurface temperatures with the Niño 3 index leading. Alternatively, it could be argued that the preceding low-frequency variability in the tropical Pacific is a manifestation of tropical Pacific decadal variability, which is captured by low-pass filtering the Niño 3.4 index, and which leads the off-equatorial SSTa. What differs substantially between the three locations chosen here is the timing of the maximum lag, which ranges from 12 months (NH) to 58 months (WP) and 65 months (SH). While the equatorial Pacific can affect the off-equatorial regions through mechanisms such as changes in winds, these operate on large spatial scales (Capotondi and Qiu 2023) and would not lead to localised changes. The reason for these strong differences in the lag timing at the three locations is not known, but there might be different mechanisms operating in those regions such as one region being more driven by surface-heat fluxes and another more by ocean dynamics. The causes for this would be interesting to explore in a future investigation. Overall, we can assume that the broader decadal IPO pattern does, at least to some degree, relate to a delayed response of off-equatorial SSTa to low-frequency equatorial Pacific SST forcing, as suggested by $G_0$. This assumption needs to be further tested dynamically, not only statistically, to quantify the extent to which this is true.

### 4.3 Results that reject $H_0$ and $G_0$

One important feature of the IPO we identified that was not consistent with either $G_0$ or $H_0$ is summary point 3, implying that the IPO is an ENSO independent, dynamical mode. While the North Pacific SSTa were positive during IPO − phases, they were negative during IPO + phases. This pattern occurred regardless of the ENSO state and included ENSO neutral years, in which significantly different North Pacific SSTa between IPO − and IPO + phases were recorded (Fig. 2j–l; summary point 3 in Table 2). This is surprising, especially as the strong similarity between the IPO − La Niña (Fig. 2g) and IPO − pattern and IPO + EP El Niño (Fig. 2e) and IPO + pattern would lead to the assumption that the North Pacific SSTa variability occurs as a result of ENSO. North Pacific SSTa play a key role in ENSO variability and triggering ENSO events. As shown by Liguori and Di Lorenzo (2019), suppressing it in coupled climate model experiments leads to substantially reduced tropical Pacific SST variability. On the other hand, during El Niño events, the Aleutian Low often deepens, leading to a cooling of the underlying ocean while the opposite occurs during La Niña (Trenberth et al. 1998). As the frequency of El Niño events changes little between IPO − and IPO + phases, this deepening likely dominates during IPO + phases due to the decreased prevalence of La Niña events and can therefore be seen in the average SSTa during IPO + phases. During IPO − phases, however, when La Niña events dominate, the weakening of the Aleutian Low is associated with a warming of the North Pacific SSTa.

Nevertheless, this does not explain the contrasting IPO −/IPO + SSTa in ENSO neutral years (Fig. 2j–l), and also does not hold up for EP El Niño events in IPO − (Fig. 2d) and La Niña events in IPO + phases (Fig. 2h) as these are accompanied by the same sign North Pacific SSTa as in the tropical Pacific. One possibility is that weaker magnitude ENSO events (e.g., for EP El Niño events in IPO − phases) or events with equatorial confined SSTa maxima (La Niña events in IPO +) have a weaker atmospheric teleconnection to the North Pacific and Indian Ocean and do not trigger an anomalous local atmospheric and/or

oceanic response. On the contrary, stronger ENSO events with a broader zonal and meridional extent of equatorial SSTa (La Niña events in IPO − and EP El Niño events in IPO + phases) also show stronger signatures in more remote regions such as the North Pacific and Indian Ocean.

Therefore, our statistical study indicates that the North Pacific SSTa are influenced by ENSO, but also behave in a way that is independent of ENSO. These results are consistent with findings by Zhao et al. (2021) who show in their sensitivity experiments that decoupling the tropical and North Pacific leads to changes in North Pacific SST variability, even though the sign of central North Pacific SSTa remains the same. This was attributed to internal dynamics in the North Pacific such as variability in the Kuroshio–Oyashio Extension region (Zhao et al. 2021) and provides an argument against $H_0$ and $G_0$ and for the IPO as a more dynamical, and hence, predictable mode of variability and a more complex null hypothesis. Other factors can dominate, and possibly also override the response to ENSO as seen for events that do force an opposite sign response in North Pacific SSTa.

Overall, much more research is required to identify the extent to which ENSO and the IPO are related, and to identify the exact causes of the IPO. Neither ENSO statistics alone ($H_0$), nor ENSO-related heat fluxes ($G_0$) can explain all of the IPO's variability. This suggests a relationship exists between ENSO and the IPO, but also ENSO independence to a degree, especially in the North Pacific. Future work should focus on the role of ENSO and other dynamical modes of variability that likely influence the IPO, as well as the influence of a changing climate on characteristics of the IPO and its relationship to anthropogenic and natural aerosols and volcanic activity.

**Supplementary Information** The online version contains supplementary material available at https://doi.org/10.1007/s00382-023-07035-8.

**Acknowledgements** Hanna Heidemann thanks the Northern Australia Climate Program, funded by Meat and Livestock Australia, the Queensland Government through the Drought and Climate Adaptation Program, the De-Risk International Climate Initiative and the University of Southern Queensland for funding her PhD scholarship. The data processing was supported by the University of Southern Queensland Fawkes HPC, which is co-sponsored by the Queensland Cyber Infrastructure Foundation. Hanna Heidemann further acknowledges the support of the National Environmental Science Programme's Earth Systems and Climate Change Hub.

**Author contributions** Hanna Heidemann has written the first draft of the manuscript, conducted all analysis and visualised them as a part of her PhD thesis. All authors contributed to the results and approved the final manuscript.

**Funding** This work was supported by the Northern Australia Climate Program, funded by Meat and Livestock Australia, the Queensland Government through the Drought and Climate Adaptation Program, the De-Risk International Climate Initiative and the University of Southern Queensland through Hanna Heidemann's PhD scholarship.

**Data availability** HadISST SST data are publicly available through the UK MetOffice: https://www.metoffice.gov.uk/hadobs/hadisst/data/download.html.

## Declarations

**Conflict of interest** The authors have no relevant financial or non-financial interests to disclose.



## References

Alexander MA, Deser C, Timlin MS (1999) The reemergence of SST anomalies in the North Pacific Ocean. J Clim 12:2419–2433. https://doi.org/10.1175/1520-0442(1999)012%3c2419:trosai%3e2.0.co;2

Ashok K, Behera SK, Rao SA et al (2007) El Niño Modoki and its possible teleconnection. J Geophys Res Ocean 112:1–27. https://doi.org/10.1029/2006JC003798

Cai W, Ng B, Geng T et al (2023) Anthropogenic impacts on twentieth-century ENSO variability changes. Nat Rev Earth Environ. https://doi.org/10.1038/s43017-023-00427-8

Capotondi A, Qiu B (2023) Decadal variability of the Pacific shallow overturning circulation and the role of local wind forcing. J Clim 36:1001–1015. https://doi.org/10.1175/jcli-d-22-0408.1

Capotondi A, Wittenberg AT, Kug JS et al (2020) ENSO diversity. In: McPhaden MJ, Santoso A, Cai W (eds) El Niño Southern Oscillation in a Changing Climate. American Geophysical Union (AGU), pp 65–86

Capotondi A, Newman M, Xu T, Di Lorenzo E (2022) An optimal precursor of Northeast Pacific marine heatwaves and Central Pacific El Niño events. Geophys Res Lett 49:e2021GL097350. https://doi.org/10.1029/2021GL097350

Choi J, Son S-W (2022) Seasonal-to-decadal prediction of El Niño–Southern Oscillation and Pacific Decadal Oscillation. NPJ Clim Atmos Sci 5:1–8. https://doi.org/10.1038/s41612-022-00251-9-00251-9

Deser C, Alexander MA, Xie S-P, Phillips AS (2010) Sea surface temperature variability: patterns and mechanisms. Annu Rev Mar Sci 2:115–143. https://doi.org/10.1146/annurev-marine-120408-151453

Di Lorenzo E, Liguori G, Schneider N et al (2015) ENSO and meridional modes: a null hypothesis for Pacific climate variability. Geophys Res Lett 42:9440–9448. https://doi.org/10.1002/2015GL066281

Di Lorenzo E, Xu T, Zhao Y et al (2023) Modes and mechanisms of Pacific decadal-scale variability. Annu Rev Mar Sci. https://doi.org/10.1146/annurev-marine-040422-084555

Dieppois B, Capotondi A, Pohl B et al (2021) ENSO diversity shows robust decadal variations that must be captured for accurate future

projections. Commun Earth Environ 2:1–13. https://doi.org/10.1038/s43247-021-00285-6
England MH, Mcgregor S, Spence P et al (2014) Recent intensification of wind-driven circulation in the Pacific and the ongoing warming hiatus. Nat Clim Change 4:222–227. https://doi.org/10.1038/nclimate2106
Freund MB, Henley BJ, Karoly DJ et al (2019) Higher frequency of Central Pacific El Niño events in recent decades relative to past centuries. Nat Geosci 12:450–455. https://doi.org/10.1038/s41561-019-0353-3
Gordon EM, Barnes EA, Hurrell JW (2021) Oceanic harbingers of Pacific Decadal Oscillation predictability in CESM2 detected by neural networks. Geophys Res Lett 48:1–11. https://doi.org/10.1029/2021GL095392
Han W, Meehl GA, Hu A et al (2014) Intensification of decadal and multi-decadal sea level variability in the western tropical Pacific during recent decades. Clim Dyn 43:1357–1379. https://doi.org/10.1007/s00382-013-1951-1
Heidemann H, Ribbe J, Cowan T et al (2022) The influence of interannual and decadal Indo-Pacific sea surface temperature variability on Australian monsoon rainfall. J Clim 35:425–444. https://doi.org/10.1175/JCLI-D-21-0264.1
Henley BJ (2017) Pacific decadal climate variability: Indices, patterns and tropical-extratropical interactions. Glob Planet Change 155:42–55. https://doi.org/10.1016/j.gloplacha.2017.06.004
Henley BJ, Gergis J, Karoly DJ et al (2015) A tripole index for the interdecadal Pacific oscillation. Clim Dyn 45:3077–3090. https://doi.org/10.1007/s00382-015-2525-1
Liguori G, Di Lorenzo E (2019) Separating the North and South Pacific meridional modes contributions to ENSO and tropical decadal variability. Geophys Res Lett 46:906–915. https://doi.org/10.1029/2018GL080320
Liu F, Zhang W, Jin FF, Hu S (2021) Decadal modulation of the ENSO–Indian Ocean basin warming relationship during the decaying summer by the interdecadal pacific oscillation. J Clim 34:2685–2699. https://doi.org/10.1175/JCLI-D-20-0457.1
Maher N, Sen GA, England MH (2014) Drivers of decadal hiatus periods in the 20th and 21st centuries. Geophys Res Lett 41:5978–5986. https://doi.org/10.1002/2014GL060527
Mantua NJ, Hare SR (2002) The Pacific decadal oscillation. J Oceanogr 58:35–44. https://doi.org/10.1023/A:1015820616384
McCreary JP, Lu P (1994) Interaction between the subtropical and equatorial ocean circulations: the subtropical cell. J Phys Oceanogr 24:466–497. https://doi.org/10.1175/1520-0485(1994)024%3c0466:IBTSAE%3e2.0.CO;2
Meehl GA, Teng H, Capotondi A, Hu A (2021) The role of interannual ENSO events in decadal timescale transitions of the Interdecadal Pacific Oscillation. Clim Dyn 57:1933–1951. https://doi.org/10.1007/s00382-021-05784-y
Newman M, Alexander MA, Ault TR et al (2016) The Pacific decadal oscillation, revisited. J Clim 29:4399–4427. https://doi.org/10.1175/JCLI-D-15-0508.1
Okumura YM, Sun T, Wu X (2017) Asymmetric modulation of El Niño and La Niña and the linkage to tropical Pacific decadal variability. J Clim 30:4705–4733. https://doi.org/10.1175/JCLI-D-16-0680.1
Power S, Colman R (2006) Multi-year predictability in a coupled general circulation model. Clim Dyn 26:247–272. https://doi.org/10.1007/s00382-005-0055-y
Power SB, Smith IN (2007) Weakening of the Walker Circulation and apparent dominance of El Niño both reach record levels, but has ENSO really changed? Geophys Res Lett 34:1–4. https://doi.org/10.1029/2007GL030854
Power S, Casey T, Folland C et al (1999) Inter-decadal modulation of the impact of ENSO on Australia. Clim Dyn 15:319–324. https://doi.org/10.1007/s003820050284
Power S, Haylock M, Colman R, Wang X (2006) The predictability of interdecadal changes in ENSO activity and ENSO teleconnections. J Clim 19:4755–4771. https://doi.org/10.1175/JCLI3868.1
Power S, Lengaigne M, Capotondi A et al (2021) Decadal climate variability in the tropical Pacific: characteristics, causes, predictability, and prospects. Science (80-) 374:1–10. https://doi.org/10.1126/science.aay9165
Qin M, Dai A, Hua W (2020) Aerosol-forced multidecadal variations across all ocean basins in models and observations since 1920. Sci Adv 6:eabb0425. https://doi.org/10.1126/sciadv.abb0425
Rayner NA, Parker DE, Horton EB et al (2003) Global analysis of sea surface temperature, sea ice, and night marine air temperature since the late nineteenth century. J Geophys Res 108:1–56. https://doi.org/10.1029/2002JD002670
Ren HL, Jin FF (2011) Niño indices for two types of ENSO. Geophys Res Lett 38:1–5. https://doi.org/10.1029/2010GL046031
Taschetto AS, Gupta AS, Hendon HH et al (2011) The contribution of Indian Ocean sea surface temperature anomalies on Australian summer rainfall during El Niño events. J Clim 24:3734–3747. https://doi.org/10.1175/2011JCLI3885.1
Timmermann A (2003) Decadal ENSO amplitude modulations: a nonlinear paradigm. Glob Planet Change 37:135–156. https://doi.org/10.1016/S0921-8181(02)00194-7
Timmermann A, An S-IS-I, Kug J-SJ-S et al (2018) El Niño–Southern Oscillation complexity. Nature 559:535–545. https://doi.org/10.1038/s41586-018-0252-6
Trenberth KE, Branstator GW, Karoly D et al (1998) Progress during TOGA in understanding and modeling global teleconnections associated with tropical sea surface temperatures. J Geophys Res Ocean 103:14291–14324. https://doi.org/10.1029/97jc01444
Vimont DJ (2005) The contribution of the interannual ENSO cycle to the spatial pattern of decadal ENSO-like variability. J Clim 18:2080–2092. https://doi.org/10.1175/JCLI3365.1
Vimont DJ, Battisti DS, Hirst AC (2001) Footprinting: a seasonal connection between the tropics and mid-latitudes. Geophys Res Lett 28:3923–3926. https://doi.org/10.1029/2001GL013435
Wilks DS (2011) Statistical methods in the atmospheric sciences, vol 100, 3rd edn. Academic Press, Cambridge
Zhang H, Clement A, Di NP (2014) The South Pacific meridional mode: a mechanism for ENSO-like variability. J Clim 27:769–783. https://doi.org/10.1175/JCLI-D-13-00082.1
Zhao Y, Newman M, Capotondi A et al (2021) Removing the effects of tropical dynamics from North Pacific climate variability. J Clim 34:9249–9265. https://doi.org/10.1175/JCLI-D-21